RESEARCH ARTICLE

Arc Fault Diagnosis Method for Brush Slip Ring System of Doubly-Fed Induction Generator Based on Image Recognition

KUN XIA[1], YIREN LIU[1], AND SHUAI YUAN[1,2]

[1]Department of Electrical Engineering, University of Shanghai for Science and Technology, Yangpu, Shanghai 200093, China
[2]National Local Joint Engineering Laboratory of High Energy Saving Motor and Control Technology, Anhui University, Hefei 230039, China

Corresponding author: Yiren Liu (212221718@st.usst.edu.cn)

ABSTRACT This article proposes a method for diagnosing arc faults in the brush slip ring system of a Doubly-Fed Induction Generator (DFIG) using image recognition technology. The aim is to achieve automatic detection and diagnosis of arc faults. The experimental process of this diagnostic method includes collecting a large amount of arc faults image sample data through an industrial camera, preprocessing the collected data, completing data annotation, and creating a dataset. Build the YOLOv5 model using the PyTorch deep learning framework, train it using the arc faults image dataset, observe the convergence of the loss function during the model training process, and analyze the model testing results, taking into account evaluation indicators such as Precision, Recall, mean Average Precision (mAP), and Frames Per Second (FPS). This article proposes the K-YOLO++ model for diagnosing arc faults. The K-YOLO++ model is an improved model obtained by adding a small object detection layer on the basis of the YOLOv5 model, improving the multi-scale detection mechanism, and executing the K-means++ clustering algorithm to improve the anchors. The test results on the experimental dataset of arc faults in the brush slip ring system of Doubly-Fed Induction Generator indicate that the K-YOLO++ network model has improved Precision, Recall, and mAP. The mAP of the improved model is 88.36%, with a FPS of 50.62. The recognition effect of small targets is superior, effectively reducing missed and false detections, enabling efficient and accurate arc faults diagnosis.

INDEX TERMS Arc fault, deep learning, image recognition, K-YOLO++, small object detection.

I. INTRODUCTION

In recent years, the manufacturing technology of variable speed constant frequency wind turbines has been widely used in megawatt models, and it is one of the hot spots of wind power research. DFIG has rapidly become the mainstream model of wind turbines due to its wide speed range, independently adjustable active and reactive power [1] and accounts for a large proportion of them. In DFIG, the brush slip ring is an important dynamic and static conversion device that plays a vital role in the stable operation of the generator. However, due to the use of brush slip ring system, the failure rate of DFIG is high and arc faults during operation is inevitable.

Arc detection can be used to judge arc faults in brush slip rings in DFIG and protect equipment. The use of image recognition methods to detect arcs on the brush slip ring can identify the arc area. By calculating the arc area, the degree of danger of arc combustion can be divided into several levels, allowing for evaluation of the degree of arc failure danger.

Research on arc faults started in the 1970s in Western countries. In recent years, many scholars and technicians of related enterprises have participated in the research of this problem. Reference [2] proposed a new arc faults detection and phase selection method based on single-phase current. Performing wavelet threshold denoising, piecewise linear fitting

and first-order differential processing on single-phase current signals to filter out noise interference and highlight fault characteristics. Apply Fractional Fourier Transform (FRFT) to first-order differential signals to construct an amplitude matrix of the signal from the time domain to the frequency domain. A low-dimensional arc faults feature vector was created by combining the two-level block singular value decomposition (SVD) method. A Support Vector Machine (SVM) model for arc faults detection and phase selection was established using Grid Search (GS) and Particle Swarm Optimisation (PSO). Reference [3] determined that a Rogowski coil could be constructed with sufficient bandwidth to cover the relevant frequency band of 1 kHz-1 MHz, found that the amplitude of the pulse and the difference in the integrated fast Fourier transform of the current signal correlated well with the series fault, described experiments to demonstrate that, over the range tested, the two parameters were robust with respect to the pressure of the atmosphere in which the arc forms, the electrode material, the speed at which the electrodes separate to initiate the arc, the switch operation, the load type and the load change, and demonstrated that, within the known limits of travelling wave localization, such localization could be used based on the electrode material, the rate at which the electrodes separate to initiate the arc, the switching operation, the load type and the load change, and showed that, within the known limits of travelling wave localization, such localization can be used based on the capacitor current pulse information after it has been validated by spectrum analysis as a fault and not a spurious signal. Reference [4] proposed a DC series arc faults detection method that comprehensively uses the information of line current and supply voltage. An experimental platform for DC fault arc generation and detection was established using a DC-DC converter and a photovoltaic power supply as DC power sources, and the proposed method was confirmed by experiments using this platform.

As research into arc faults deepens, the indicator method has poor performance in processing non periodic signals, limited resolution, and computational complexity. The shortcomings of wavelet analysis method, such as high computational complexity, difficult parameter selection, and high technical threshold, became increasingly apparent.

Consequently, many scholars were opting to develop arc detection models and study arc faults by using parameters such as voltage and current. Reference [5] described the characteristics of arc signals using sparse coding and conducts intelligent feature learning and classification through neural network. The methodology is elaborately structured by a pretreatment layer, a sparse representation layer, and a decision layer. Reference [6] presented an adaptive arc faults diagnosis model that discretizes continuous time series based on half cycle length and performs adaptive matrix transformation on the discrete sequence using convolution operation. During the training phase, an adaptive asymmetric convolution kernel was designed based on the data

distribution characteristics of the encoding matrix. This design effectively mines continuous time information and related information in the time domain. Reference [7] established a multi-characteristic arc model based on the volt-ampere characteristics, current sag characteristics, and power spectrum characteristics of arc faults. The principle for selecting arc detection points has been formed based on the frequency domain characteristics of arc faults and the interaction between different branches. Reference [8] proposed a method for detecting series arc faults based on a high-frequency (HF) RLC arc model and a one-dimensional convolutional neural network (1DCNN). The method uses a current transformer (D-HFCT) to receive differential HF features and simplify currents with complex features into different types of oscillation signals. The 1DCNN model is trained using simulated data and can detect series arc faults under different types of actual loads. Reference [9] analyzed several typical loads, including nonlinear and complex loads such as power electronic loads, and selected five time-domain parameters of the current for arc faults detection: average value, median value, variance value, RMS value, and distance of the maximum and minimum values. The study employed various machine learning algorithms for arc faults detection and compared their detection accuracies. Reference [10] proposed a method for extracting AC series arc faults features based on the Wigner-Hough transform. The method selects the WHT peak change ratios of current in adjacent periods as the features and uses the natural gradient lifting algorithm (NG-Boost) for state judgment. However, such methods also have certain limitations, including high false alarm rates, low detection accuracy, significant environmental impact, and high costs.

Other literatures focus on using the high-frequency electromagnetic radiation signal during arc occurrence as the detection standard. Reference [11] proposed a new method for detecting arc flash faults using spectroscopy. Copper and aluminum are used as conductors, and when an arc occurs, the optical spectrometer measures and records the spectra of both materials. This allows for accurate and rapid detection of arc flash. But this method has problems such as being greatly affected by the environment, limited detection sensitivity, background noise interference, and complex data processing.

Image recognition is a technology that utilizing computer resources to process and analyze target images, classifying them into objects within the scope of human cognition. The development stages of image recognition can be divided into text recognition, ordinary digital image processing recognition, and object recognition [12]. Nowadays, image recognition has been widely applied in many fields and has achieved significant results. Therefore, this article proposes to apply image recognition technology to the diagnosis of arc faults in the brush slip ring system of a DFIG.

Reference [13] proposed a lightweight model, YOLO5_ CA, based on YOLOv5 for the automatic detection of helmet-wearing by construction workers. The detection accuracy in complex scenes can be enhanced by extracting

key information and suppressing non-key information. Reference [14] proposed an intelligent detection algorithm called Swin Transformer Attention Efficient Algorithm (STAE-YOLO) that enables real-time monitoring of construction machinery and equipment around transmission lines and rapid identification of potential risks. Reference [15] introduced an efficient and lightweight GPR pavement disease image recognition algorithm based on the YOLOv4 object detection algorithm. This is achieved by combining MobileNetV2 and CBAM attention mechanisms and using the Focal loss confidence loss function to iterate the model. Reference [16] proposed the Improved YOLO algorithm for real-time recognition of strawberry seedling flowers and fruits in greenhouses. The article proposes using GS Conv to construct a network neck GS-ELAN optimization module to suppress shallow noise interference from high-resolution prediction heads and alleviate the parameter increase caused by high-resolution prediction heads. Additionally, it referenced a modified, lightweight deep object detection model based on the YOLO-v5 architecture in reference [17]. It achieved this by using a multi-scale mechanism to learn deep discriminative feature representations at different scales and automatically determine the most suitable scales for detecting objects in a scene. The model proposed in reference [18], called ''YOLO with lightweight feature fusion network (LFF-YOLO).'' can detect objects of varying sizes, including large, small, and tiny objects. The model employs ShuffleNetv2 as a feature extraction network to reduce the number of parameters. The proposed model introduces the lightweight feature pyramid network (LFPN) to enhance the efficiency of multi-scale feature fusion. Additionally, the adaptive receptive field feature extraction (ARFFE) module is employed to generate multi-receptive field information by weighting the multi-receptive field channels. Reference [19] presented the YOLO-class model, which is transferred to optimize the detection of small, dense, and occluded targets through the YOLO-Extract model. Representative Batch Normalization and Mish activation functions were used to optimize the Conv module. VariFocal loss was used to optimize the classification loss function to improve accuracy caused by imbalanced data samples. Finally, RepVGG modules were designed in the Backbone to further improve the model's detection accuracy. Reference [20] presented a lightweight attention-guided YOLO with a level set layer (LA-YOLO-LLL) for landslide detection from optical satellite images. The MobileNetv3 replaced the original backbone of YOLO to reduce parameter complexity and improve model transferability. To improve landslide detection performance, a light pyramid feature reuse fusion attention mechanism was presented. The YOLO head integrated a level set layer to produce accurate landslide boundaries. Reference [21] presented a new lightweight network with feature relay amplification and multiscale feature jump connection structure designed to extract features of each scale target in SAR images, improving recognition and localization. Additionally, the K-Means method is used to obtain the target scale distribution, allowing for the selection

of more appropriate preset anchor boxes and reducing network learning difficulty. RoI Align is used instead of region of interest (RoI) Pooling to reduce quantization error during positioning. Reference [22] employed an algorithm of adaptive model-driven clustering to initialize a model of an elongated object with a data-driven process on local partial detections. The model is then refined iteratively by model-driven clustering and data-driven model updating on the outputs of the Faster-RCNN and DCNN. This method utilizes Faster-RCNN to produce reliable partial detections and model-driven clustering to create a comprehensive representation, resulting in the generation of a precise oriented bounding box for elongated object detection.

Currently, research on the diagnosis of arc faults in DFIG brush slip ring systems is scarce both domestically and internationally, and existing detection methods still have deficiencies in accuracy, timeliness, and practicality. In addition, no relevant research has been found on the application of image recognition technology to arc faults detection in DFIG brush slip ring systems. Therefore, this article will conduct in-depth research on the diagnosis of arc faults in DFIG brush slip ring systems based on image recognition technology. The main contributions of this article are as follows:

1) This article proposes to apply image recognition technology to the field of arc faults diagnosis in DFIG brush slip ring systems.
2) This method can effectively and accurately identify arc faults generated by DFIG brush slip ring systems, and can classify the level of arc faults.
3) Compared with traditional detection methods, this method is simple to operate, cost-effective, and has accurate detection results.

II. BASIC PRINCIPLES OF THE SYSTEM
A. THE OCCURRENCE OF ARC FAULTS
A brush slip ring system for a megawatt-level DFIG primarily comprises of brushes and slip rings enclosed in a sealed box. It employs three-phase excitation slip rings and six uniformly distributed brushes. However, this article focuses on studying the single-phase arc faults of the DFIG brush slip ring system due to the convenience of laboratory environment, experimental platform construction, and experimental repeatability.

Arcs can be classified into three types: series arc, parallel arc, and grounding arc, based on their generation methods. In the DFIG brush slip ring system, the most common type of arc faults is the series arc. This type of fault occurs due to the principle of gas discharge. It is important to note that dry air, despite being a good insulator, can still lead to the occurrence of a series arc faults. Applying voltage to both ends of the gas causes breakdown and ionization of the air between the electrodes. This generates a current that passes through the gap between the conductors, resulting in arc faults. Figure 1 shows the schematic diagram of the arc faults.

If the electric field applied to the brush slip ring system exceeds the dielectric breakdown strength of the medium, it will quickly transition from a non-conductive to an
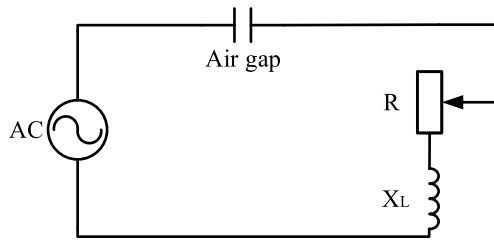
FIGURE 1. Arc faults schematic diagram.

electrical state. This can result in arc faults on the brush slip ring system, as shown in Figure 2.
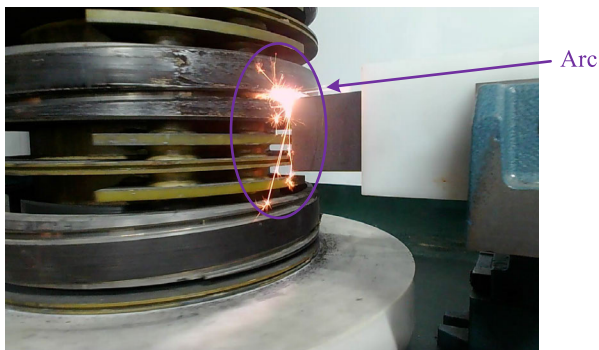

FIGURE 2. Arc faults of the brush slip ring system.

Arc faults in the brush slip ring system can occur due to unstable contact during installation, resulting in small gaps in the rotor circuit.

1) This increases the contact resistance of that phase, forcing the current shared by other phase brushes and slip rings to increase, leading to excessive current and resulting in arc faults. This increases the contact resistance of that phase, forcing the current shared by other phase brushes and slip rings to increase, leading to excessive current and resulting in arc faults. The overheating and deformation of the brushes due to surface burns can also be a consequence of these faults.

2) When the brush slip ring system operates for an extended period with the wind turbine generator set, mechanical wear occurs between the brush and slip ring due to long-term friction. This wear causes an increase in the amount of carbon powder produced, leading to uneven contact between the brush and slip ring surface. During the wind turbine generator set's power generation state, an arc fire may be pulled out on the brush and slip ring surface, which can burn related equipment.

3) The brush slip ring system of the DFIG is located in a confined space, making it difficult to dissipate the heat generated during wind turbine operation. This high temperature can cause the spring tension on the brush to degrade, resulting in gaps. The gas present in the gaps can cause a continuous arc effect due to thermal

ionization. This can lead to the formation of electric burns on the surface of the slip ring and brush, which can further increase the mechanical wear of the brush and slip ring, thereby posing greater safety hazards.

If the contact between the brush and the slip ring is poor, current leakage and electric sparks may occur in the DFIG. Continuing to operate the DFIG under these conditions will cause the electric sparks to discharge, resulting in arc faults. This can eventually burn out the brush and slip ring, as shown in Figure 3. Such a situation can affect the normal operation of wind turbines and may even cause shutdown accidents in severe cases.
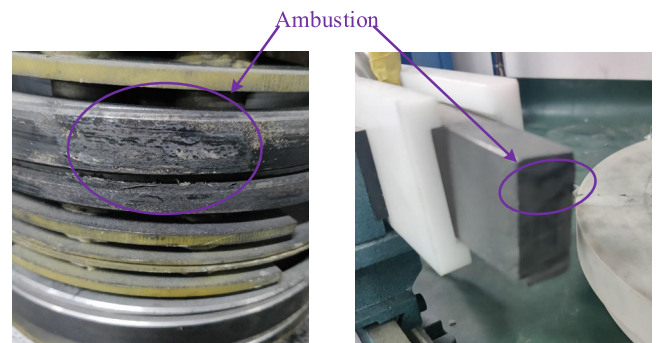
FIGURE 3. Ambustion of brush slip rings caused by arc faults.

The intensity of ambustion on the surface of the DFIG brush slip ring increases with the continuous occurrence of arc faults. It is crucial to diagnose and determine accurate results in the early stages of arc faults to prevent a vicious cycle.

The fundamental cause of arc faults in the DFIG brush slip ring system is the gap between the brush and slip ring. In future experiments on arc detection in DFIG brush slip ring systems, the distance between the brush and slip ring can be adjusted to intentionally create arc faults on the experimental platform.

B. INTRODUCTION TO EXPERIMENTAL PLATFORM

By analyzing the working principle of DFIG and the mechanism of AC series arc faults, as well as considering the convenience of laboratory environment, experimental platform construction, and experimental repeatability, this article mainly studies the single-phase arc faults of DFIG brush slip ring system. The DFIG rotor feeding system was reformed and replaced, the wiring method was changed, the three-phase system was adjusted to a single-phase system, and the output link of the wind turbine was replaced with an equivalent load to simulate the actual operating conditions of the brush slip ring system. An experimental platform for DFIG brush slip ring system arc faults diagnosis was designed based on image recognition, and its schematic diagram is shown in Figure 4.

The experimental platform for diagnosing arc faults in DFIG brush slip ring systems based on image recognition consists of two parts: arc faults occurrence device and arc

and comparable detection accuracy, making it more suitable for scenarios that require real-time arc faults diagnosis.

Figure 6 displays the network structure of the YOLOv5 [25] algorithm. A typical target detection algorithm comprises four general modules: Input, Backbone network, Neck network, and Head. The YO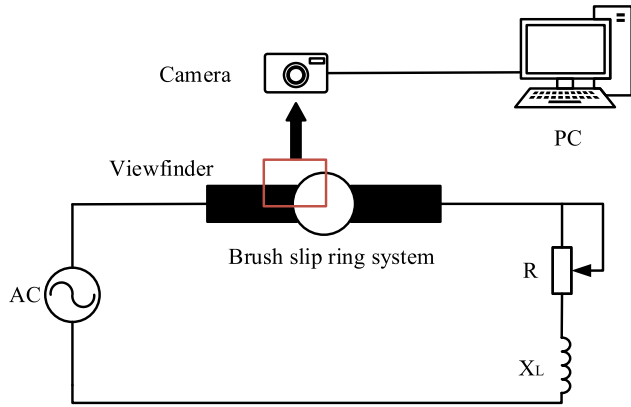LOv5 algorithm has four versions: YOLOv5s, YOLOv5m, YOLOv5l, and YOLOv5x. This article uses YOLOv5s, while other versions expand and enhance the network based on YOLOv5s.

FIGURE 6. YOLOv5 network architecture.

Input: The network's input image size is 640×640. Typically, this stage involves an image preprocessing step, which scales the input image to the network's input size and performs operations such as normalization.

Backbone network: The YOLOv5's backbone feature extraction network is a convolutional neural network that extracts arc image features. Its main structure comprises the Focus, CBS module, C3 module, and SPPF module. The Focus structure performs slicing operations on the image and merges it with a Concat layer to increase the number of channels in the arc image. The CBS module includes convolution, batch normalization, and SiLU activation functions. These functions can achieve faster and more efficient feature extraction compared to ordinary convolutions. The C3 module, built using the CSPNet concept, ensures effective feature extraction of the backbone network while also addressing the problem of gradient explosion in the network. The SPPF module is a fast implementation of the SPP module. It maximizes input features by adopting three similar concatenated max pooling layers and achieves multi-scale feature fusion through feature concatenation.

Neck network: The combination of FPN and PAN structures in the Neck network enhances the diversity and robustness of features. FPN structure generates multiple feature maps of different scales to detect targets of different scales by upsampling the output feature maps generated through multiple convolutional downsampling operations in the backbone network. The top-down feature fusion process of FPN improves its feature fusion ability. Based on this approach, the PAN structure is combined with a bottom-up

FIGURE 4. Principle diagram of DFIG brush slip ring system arc faults diagnosis experimental platform.

faults detection device. The arc faults occurrence device comprises an AC power supply that is adjustable for both frequency and voltage, a brush slip ring system, and an equivalent load. In a sub-synchronous state, the AC power supply simulates the power grid to provide AC power of varying amplitudes and frequencies to the rotor side. This is achieved by using adjustable reactance and inductance to simulate the rotor winding. In the ultra-synchronous state, the AC power supply simulates the AC input on the rotor side, while the adjustable reactance and inductance simulate the load on the grid side. The device for detecting arc faults comprises a camera and a computer. These are used to collect the arc faults image dataset of the DFIG brush slip ring system. Figure 5 shows the structure of the experimental platform.
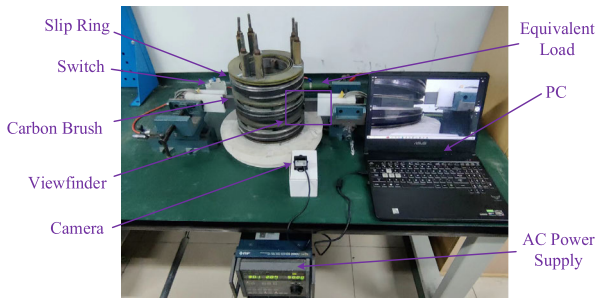

FIGURE 5. Diagram of DFIG brush slip ring system arc faults diagnosis experimental platform.

III. PRINCIPLE OF YOLOv5 ALGORITHM
In order to meet the real-time requirements of arc faults diagnosis, this article chooses a one-stage object detection algorithm with faster detection speed for experimentation. YOLOv5 is an efficient object detection algorithm. Compared to YOLOv1 to YOLOv4, YOLOv5 has advantages such as faster inference speed, higher accuracy, simpler code structure, and support for lightweight deployment. Compared with updated object detection algorithms such as YOLOv8 [23] and YOLOv9 [24], the YOLOv5 model has a smaller volume, fewer parameters, less computational resources and training inference time, faster training speed,

feature fusion path, resulting in improved accuracy of the network model for targets of varying scales.

Head: The head of an object detection algorithm is primarily responsible for determining the position and category of the target object. It typically includes a classification branch and a regression branch, with the number of branches varying depending on the detection algorithm used. YOLOv5, for instance, uses the CIoU Loss function instead of the Smooth L1 Loss function to estimate the position loss of bounding boxes [26], resulting in improved detection accuracy. This module comprises three detection heads with scales of 20×20, 40×40, and 80×80 to detect targets of varying sizes.

The YOLO series models are preferred for arc faults diagnosis tasks due to their real-time requirement and fast detection speed. Among the YOLO series models, the YOLOv5 network model is lightweight and has a fast detection speed, making it suitable for deployment on embedded devices. However, the real-time detection of small targets in the DFIG brush slip ring system cannot meet daily industrial needs due to its complexity and the small fault arc target. Therefore, this article presents an improved YOLOv5 model for diagnosing arc faults in the DFIG brush slip ring system.

IV. METHODS FOR MODEL IMPROVEMENT

A. SMALL OBJECT DETECTION LAYER

The initial phase of arc faults is crucial for its identification. During this phase, the arc shape is typically small, making it essential for the arc faults diagnosis network model to have the ability to identify small targets. In the feature extraction process of the YOLOv5 network model, some information may be lost due to multiple convolution, pooling, and other operations, resulting in poor detection performance of the model for small targets. Therefore, this article proposes adding a small object detection layer to YOLOv5's multi-scale detection to enhance the model's ability to recognize small targets.

It is important to note that increasing the number of detection layers will also increase the number of parameters in the network model, which may result in a decrease in detection speed. To meet the accuracy and real-time requirements of the arc faults diagnosis model, this article added a 160×160 detection layer to the output part of the YOLOv5 network model. Four different sized feature maps are used to identify large, medium, and small targets in the image. The improved multi-scale detection layer is shown in Figure 7. The detection layer that has been recently added performs upsampling on the 80×80 feature map to obtain a 160×160 feature map. This feature map is then connected to the 160×160 feature map in the backbone network.

B. IMPROVED ANCHORS ADJUSTMENT

The YOLOv5 algorithm performs regression prediction of the final detection box based on pre-set anchor sizes. The accuracy of the algorithm's detection is directly affected by

FIGURE 7. YOLOv5 network architecture with small object detection layer.

the anchor sizes. In the YOLOv5 algorithm, anchor sizes are obtained by clustering the target size of the COCO dataset [27] using the K-means algorithm. However, this method may not be perfectly adapted to the precise detection of arc faults in the DFIG brush slip ring system. The quality of clustering results in the K-means algorithm is directly affected by the selection of initial clustering centers, which can be sensitive to noise points, boundary points, and isolated points. To avoid possible local optima, this article employs the K-means [28] algorithm to cluster anchors, improving their adaptability. The main difference between the K-means++ algorithm and the K-means algorithm is the determination of initial cluster centers. The K-means algorithm randomly selects cluster centers, whereas the K-means++ algorithm calculates the probability of a sample point becoming the next sample center point based on its distance from the current sample point to the sample center point. It selects the sample point with the highest probability as the next cluster center and sequentially selects K cluster centers. The algorithmic process is as follows.

1) Randomly determine the first cluster center point C_1;
2) Calculate the shortest distance $D(x)$ from each sample point to the cluster center point;
3) Calculate the probability of each sample point becoming the next cluster center point based on the shortest distance from the sample point to the cluster center point $\frac{D(x)^2}{\sum_{x \in X} D(x)^2}$, and select the sample point with the highest probability as the new cluster center;
4) Repeat steps (2) and (3) until K cluster centers are extracted;
5) Calculate the distance from each sample p_k in the dataset to K cluster centers, and assign it to the class corresponding to the cluster center with the smallest distance;
6) For each category C_i, recalculate its cluster center $C_i = \frac{1}{|C_i|} \sum_{x \in C_i} X$;
7) Repeat steps 4 and 5 until the position of the cluster center no longer changes.

Output: K cluster centers $\{C_1, \ldots, C_K\}$.

The regression calculation formula for YOLOv5's target box is as follows.

$$b_x = 2\sigma(t_x) - 0.5 + c_x \tag{1}$$
$$b_y = 2\sigma(t_y) - 0.5 + c_y \tag{2}$$
$$b_w = p_w \times (2\sigma(t_w))^2 \tag{3}$$
$$b_h = p_h \times (2\sigma(t_h))^2 \tag{4}$$

Among them, (b_x, b_y, b_w, b_h) represents the center point coordinates, width, and height of the prediction box, (c_x, c_y) represents the upper left corner coordinates of the grid where the center point of the prediction box is located, (t_x, t_y) represents the offset of the center point of the prediction box from the upper left corner coordinates of the grid, (t_w, t_h) represents the scaling ratio of the width and height of the prediction box relative to the width and height of the anchors, and (p_w, p_h) represents the width and height of the anchors.

In order to constrain the center point of the prediction box to the current grid, the Sigmoid function is used to process the offset, keeping the predicted offset value within the range of (0, 1) (0, 1) (0, 1) (0, 1).

In this way, according to the regression calculation formula of the target box, the offset of the predicted box center point coordinate remains within the range of (-0.5, 1.5) (-0.5, 1.5) (-0.5, 1.5).

The YOLOv5 model is required to detect targets in 3 different scales, with each scale being assigned 3 anchor sizes for prediction, resulting in a total of 9 anchors. Table 1 illustrates the matching between the initial anchors and the feature maps set by the YOLOv5 network model.

TABLE 1. Anchors of YOLOv5 network model.

Feature Maps	Anchors		
20×20	10×13	16×30	33×23
40×40	30×61	62×45	59×119
80×80	116×90	156×198	373×326

The improved detection layer matches a total of 12 anchors based on the feature maps of each scale, resulting in K=12 clusters. The K-YOLO++ network model, which uses the K-means++ algorithm for anchor clustering, can output feature maps of 4 different sizes. Table 2 shows the matching situation between the improved anchors and the feature maps.

TABLE 2. Anchors of K-means++ algorithm clustering.

Feature Maps	Anchors		
20×20	20×23	32×38	49×57
40×40	56×101	93×90	84×162
80×80	147×148	146×222	325×235
160×160	**179×363**	**247×271**	**329×401**

V. EXPERIMENTAL DESIGN AND RESULT ANALYSIS
A. EXPERIMENTAL ENVIRONMENT
The experimental environment for this article utilized a Windows 10 64-bit operating system, an NVIDIA GeForce RTX3090 with 24GB of video memory. The Python language was used in conjunction with the CUDA11.8 GPU acceleration library and Pytorch2.01 deep learning framework. The experimental code was built using PyTorch and the training stage was conducted on a Windows 10 operating system with Python3.8 and PyTorch2.01. The model was trained for 300 epochs with a batch size of 16 and default parameters were used. The model's default input size is 640×640 pixels. Once the dataset image is scaled, it is sent to the network for training. Inference and calculations are performed on an NVIDIA GeForce RTX3090 in a Windows 10 environment.

B. MODEL TRAINING
The research data was obtained from the DFIG brush slip ring system arc faults diagnosis experimental platform in the laboratory. Figure 8(a) displays the arc images, which suffer from reduced image quality due to the spark splash produced by arc combustion. Preprocessing of the arc faults image is necessary before feature extraction to facilitate subsequent image processing.
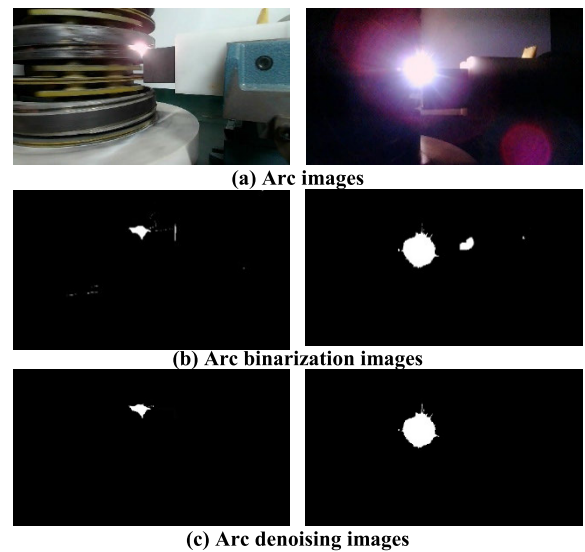

(a) Arc images

(b) Arc binarization images

(c) Arc denoising images

FIGURE 8. Arc image preprocessing.

The fault arc images were binarized resulting in only two gray values, 0 and 255, and two colors, black and white. The Otsu method was used to binarize and denoise the images, as shown in Figure 8(b) and (c).

During arc combustion, the shape and structural characteristics of the arc, including its area, long axis, and short axis, will change in response to changes in combustion intensity. This study categorizes risk into four levels based on the size of the arc area in the collected image. Level 1 is assigned when the arc image area is less than 2e3, level 2 when the arc area is greater than 2e3 and less than 6e3, level 3 when the arc area is greater than 6e3 and less than 1e4, and level 4 when the arc area is greater than 1e4.

The OpenCV library is utilized to extract area data of the faulty arc in the image, as depicted in Figure 9. The collected

FIGURE 9. Extracting area data of fault arcs.

dataset is then classified into four levels, namely level 1, level 2, level 3, and level 4, based on the area classification standard mentioned earlier. Classification labels for the arc faults image dataset are created using Labelimg software. The experiment collected more than 3000 images of arc faults at different levels, with each category containing approximately 900 images. The K-YOLO++ model was used to train and predict the classified dataset, with a ratio of 8:1:1 for the number of training, validation, and testing sets. The predicted results were used to assess the risk level of arc faults. Table 3 shows the amount of data for each level included in the arc faults dataset.

TABLE 3. Partition of arc faults dataset.

Level	Training set	Validation set	Test set
Level1	712	89	89
Level2	728	91	91
Level3	710	89	89
Level4	731	92	92

The YOLOv5 network model's training parameters dictate specific settings for model training during the training stage, as shown in Table 4. To increase sample diversity in the arc faults data, this research applies data enhancement techniques to the images input into the network model, including scale changes, left-right flips, and mosaic data enhancement.

TABLE 4. Model training hyperparameter settings.

Hyperparameter	Set value	Meaning
Batch size	16	The number of trainings samples in a batch
Epochs	300	Total number of iterations
Optimizer type	SGD	Optimizer types
Momentum	0.937	Momentum parameters in optimization methods
Lr decay type	Cos	Learning rate decline way methods
weight decay	0.0005	Weight attenuation coefficient
Label_smoothing	0	Label smoothing parameter
Init_lr	0.01	Initial maximum learning rate of the model
Min_lr	0.0001	Minimum learning rate of model

Figure 10 shows the training and prediction process of the K-YOLO++ model in the experiment.
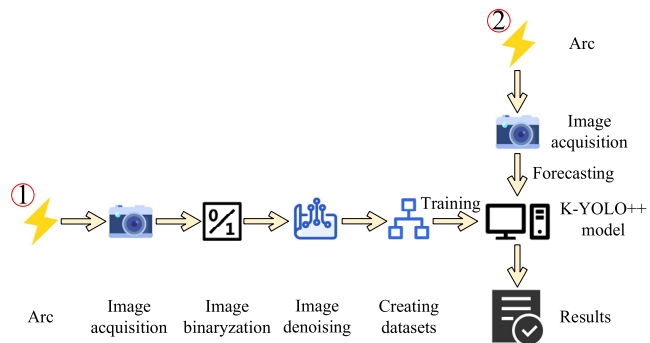

FIGURE 10. Training and prediction flowchart of K-YOLO++ model.

C. RESULTS ANALYSIS

This study uses Precision (P), Recall (R), mean Average Precision (mAP, confidence=0.5) and Frames Per Second (FPS) as evaluation indices for the model.

YOLOv5 uses CIoU as the default method for calculating bounding box loss. CIoU is based on DIoU and takes into account the aspect ratio of the bounding box.

DIoU considers factors such as distance, overlap rate, and scale between the predicted box and the actual box, making the regression of the target box more stable. Its loss calculation formula is (5).

$$L_{DIoU} = 1 - IoU + \frac{\rho^2\left(b, b^{gt}\right)}{c^2} \tag{5}$$

where b and b^{gt} represent the center points of the predicted and true boxes, ρ represents the Euclidean distance between the two center points, and c represents the diagonal distance of the minimum closure region of the predicted and true boxes.

CIoU introduces an influence factor, denoted by αv, in addition to the penalty term of DIoU. This factor considers the aspect ratio of the predicted box and the actual box. The penalty term of CIoU can be expressed as (6).

$$R_{CIoU} = \frac{\rho^2\left(b, b^{gt}\right)}{c^2} + \alpha v \tag{6}$$

Among them, α is the weight parameter, and its expression is (7).
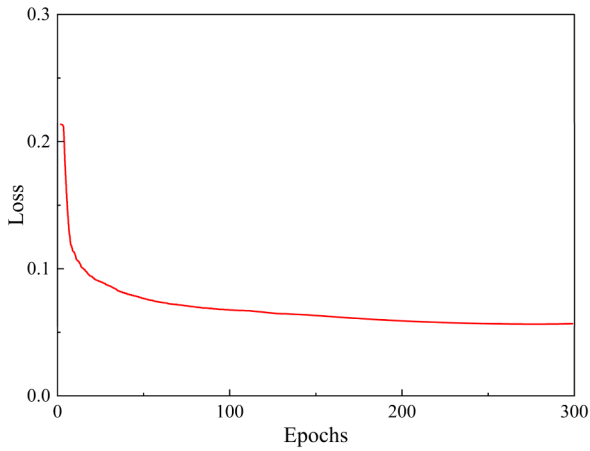
$$\alpha = \frac{v}{(1 - IoU) + v} \tag{7}$$

v is used to measure the consistency of aspect ratio, and its expression is (8).

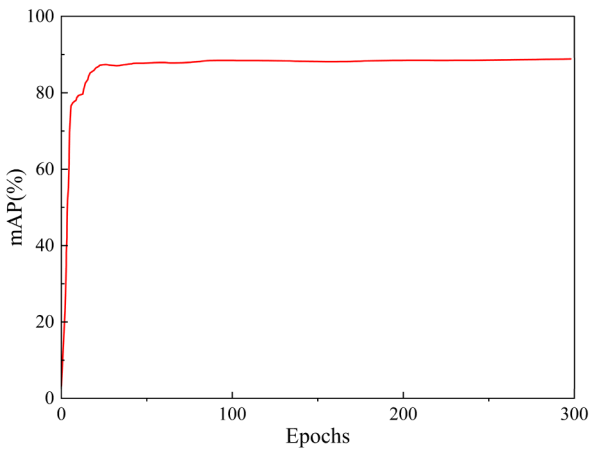$$v = \frac{4}{\pi^2}(arctan\frac{w^{gt}}{h^{gt}} - arctan\frac{w}{h})^2 \tag{8}$$

The formula for calculating loss for CIoU is (9).

$$L_{CIoU} = 1 - IoU + \frac{\rho^2\left(b, b^{gt}\right)}{c^2} + \alpha v \tag{9}$$

Figure 11 illustrates the training process of the K-YOLO++ network model. Figure 11(a) displays the loss function's variation curve during training rounds. The value

(a) Loss function curve

(b) mAP curve

FIGURE 11. Training results of K-YOLO++ network model.

TABLE 5. Performance evaluation results of network models.

Models	Level	Precision/%	Recall/%	mAP/%	FPS
Faster-RCNN	Level1	87.21	72.78	68.29	11.27
	Level2	88.16	73.27		
	Level3	84.98	70.35		
	Level4	90.23	75.42		
YOLOv3	Level1	84.26	73.03	83.65	44.26
	Level2	85.71	74.14		
	Level3	81.59	71.16		
	Level4	87.55	76.83		
YOLOv5	Level1	86.35	74.27	85.33	51.41
	Level2	88.34	75.66		
	Level3	84.82	72.34		
	Level4	89.65	78.58		
K-YOLO++	**Level1**	**95.58**	**80.88**	**88.36**	50.62
	Level2	**96.87**	**82.76**		
	Level3	**93.62**	**78.75**		
	Level4	**98.46**	**86.11**		

optimizes in multiple aspects. As a leader in one-stage object detection algorithms, YOLOv3 abandons the tedious steps of generating candidate regions in traditional object detection algorithms and instead adopts a direct regression method, while outputting the probability of target categories and
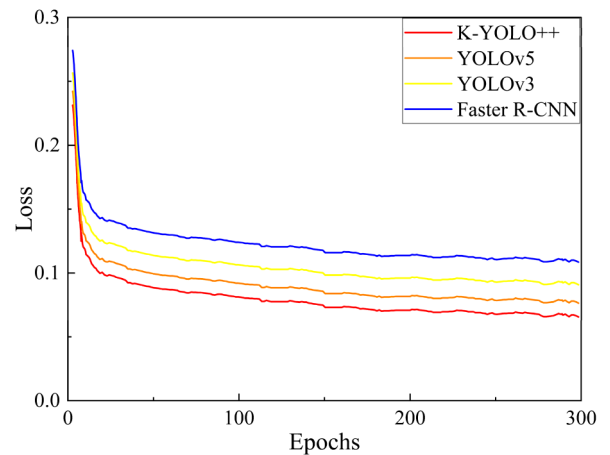
(a) Loss function curve

(b) mAP curve

FIGURE 12. Training results of the 4 network models.

of the loss function converges between 0.05 and 0.08 after 300 rounds of model training. Figure 11(b) shows the mAP variation curve with training rounds. After approximately 100 rounds of training, the mAP fluctuates less and then stabilizes.

To assess the impact of the proposed algorithm on model performance, we compared the K-YOLO++ network model with Faster-RCNN, YOLOv3, and YOLOv5.

Faster R-CNN, as a two-stage object detection algorithm, is divided into two steps to perform object classification and candidate region generation. Firstly, the algorithm extracts features from the input image and generates a feature map. These feature maps are not only passed to the classification layer for target category judgment, but also fed into the Region Proposal Network (RPN). RPN is responsible for adjusting the position of candidate regions and classifying them again.

YOLOv3, as one of the iconic algorithms in the YOLO series, has won widespread recognition in the industry due to its excellent performance and ease of use. As an upgraded version of YOLOv1 and YOLOv2, YOLOv3 not only inherits the advantages of the previous generation model, but also
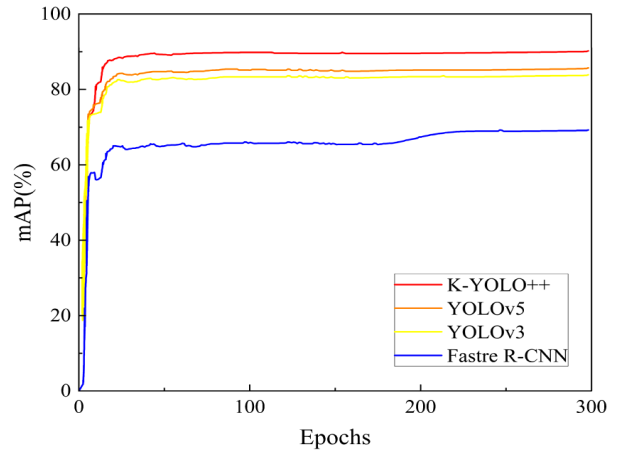
accurate prediction boxes. This innovative design significantly improves the detection speed of the model, enabling it to demonstrate excellent performance in processing real-time object detection tasks.

Table 5 presents the performance evaluation results for each network model.

Table 5 shows that K-YOLO++ outperforms Faster R-CNN, YOLOv3, and YOLOv5 in terms of Precision, Recall, and mAP. Specifically, K-YOLO++ has a 20.07% higher mAP and a 39.35 fps faster than Faster R-CNN. Additionally, K-YOLO++ has a 4-point increase in mAP compared to YOLOv3. The Precision and mAP of the K-YOLO++ have significantly increased compared to YOLOv5. The FPS has also increased by 6.36. Figure 12 shows the loss curves and mAP curves of the 4 network models.

Experiments were conducted using the collected arc faults dataset to test the performance of the K-YOLO++ network model. Figure 13 displays the recognition effect, indicating that the K-YOLO++ network model can accurately identify fault arcs with a confidence level of over 0.8 for each level. Figure 13 displays the recognition effect, indicating that the K-YOLO++ network model can accurately identify fault arcs with a confidence level of over 0.8 for each level. Figure 13 displays the recognition effect, indicating that the K-YOLO++ network model can accurately identify fault arcs with a confidence level of over 0.8 for each level. Additionally, it effectively eliminates interference from objects such as brush holders and brush boxes on the test platform.
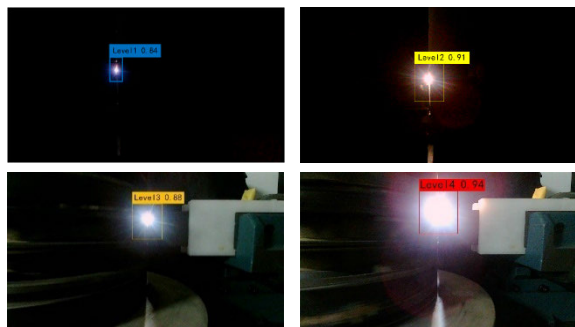

FIGURE 13. Recognition results.

VI. CONCLUSION

This article proposes an image recognition-based arc faults diagnosis method for DFIG brush slip ring systems by studying the feature extraction network, small object detection, and anchor mechanism of the YOLOv5 network model. The article proposes an improved algorithm, K-YOLO++, based on YOLOv5 to address the problems of small target scale, insufficient feature extraction ability, complex background, serious false positives, and missed detections in arc faults images. A small object detection layer was added to the original YOLOv5 network model and the K-Means++ clustering algorithm was used to obtain anchor sizes. The experimental

results indicate that the K-YOLO++ network model has a precision of 95.58%, recall of 80.88%, mAP of 88.36%, and a detection frame rate of 50.62 fps on the experimental dataset, demonstrating improved recognition performance for small targets. The aim of this study was to improve the recognition performance of arc faults images. The next step is to expand the existing arc faults dataset to enhance the image information learned by the network model. The experiment demonstrates that the algorithm proposed in this article has several advantages, including high accuracy and strong real-time performance.

REFERENCES

[1] P. Wang, Z. Zhang, Q. Huang, N. Wang, X. Zhang, and W.-J. Lee, "Improved wind farm aggregated modeling method for large-scale power system stability studies," *IEEE Trans. Power Syst.*, vol. 33, no. 6, pp. 6332–6342, Nov. 2018.

[2] H. Gao, Z. Wang, A. Tang, C. Han, F. Guo, and B. Li, "Research on series arc fault detection and phase selection feature extraction method," *IEEE Trans. Instrum. Meas.*, vol. 70, pp. 1–8, 2021.

[3] Q. Xiong, X. Feng, A. L. Gattozzi, X. Liu, L. Zheng, L. Zhu, S. Ji, and R. E. Hebner, "Series arc fault detection and localization in DC distribution system," *IEEE Trans. Instrum. Meas.*, vol. 69, no. 1, pp. 122–134, Jan. 2020.

[4] Q. Lu, Z. Ye, M. Su, Y. Li, Y. Sun, and H. Huang, "A DC series arc fault detection method using line current and supply voltage," *IEEE Access*, vol. 8, pp. 10134–10146, 2020.

[5] Y. Wang, F. Zhang, and S. Zhang, "A new methodology for identifying arc fault by sparse representation and neural network," *IEEE Trans. Instrum. Meas.*, vol. 67, no. 11, pp. 2526–2537, Nov. 2018.

[6] T. Zhang, R. Zhang, H. Wang, R. Tu, and K. Yang, "Series AC arc fault diagnosis based on data enhancement and adaptive asymmetric convolutional neural network," *IEEE Sensors J.*, vol. 21, no. 18, pp. 20665–20673, Sep. 2021.

[7] W. Miao, Z. Wang, F. Wang, K. H. Lam, and P. W. T. Pong, "Multi-characteristics arc model and autocorrelation-algorithm based arc fault detector for DC microgrid," *IEEE Trans. Ind. Electron.*, vol. 70, no. 5, pp. 4875–4886, May 2023.

[8] R. Jiang, Y. Wang, X. Gao, G. Bao, Q. Hong, and C. D. Booth, "AC series arc fault detection based on RLC arc model and convolutional neural network," *IEEE Sensors J.*, vol. 23, no. 13, pp. 14618–14627, Jul. 2023.

[9] H.-L. Dang, J. Kim, S. Kwak, and S. Choi, "Series DC arc fault detection using machine learning algorithms," *IEEE Access*, vol. 9, pp. 133346–133364, 2021.

[10] J. Wang, Y. Liu, Y. Zhao, and Q. Yang, "Research on AC arc fault detection method based on Wigner-Hough transform and NG-boost," in *Proc. IEEE 4th Int. Conf. Electr. Mater. Power Equip. (ICEMPE)*, May 2023, pp. 1–4.

[11] L. Zhao, Y. Zhou, K.-L. Chen, S.-H. Rau, and W.-J. Lee, "High-speed arcing fault detection: Using the light spectrum," *IEEE Ind. Appl. Mag.*, vol. 26, no. 3, pp. 29–36, May 2020.

[12] Y. Ai, C. Lei, J. Cheng, and J. Mei, "Prediction of weld area based on image recognition and machine learning in laser oscillation welding of aluminum alloy," *Opt. Lasers Eng.*, vol. 160, Jan. 2023, Art. no. 107258.

[13] X. Wu, S. Qian, and M. Yang, "Detection of safety helmet-wearing based on the YOLO_CA model," *Comput., Mater. Continua*, vol. 77, no. 3, pp. 3349–3366, 2023.

[14] C. Ji, F. Zhang, X. Huang, Z. Song, W. Hou, B. Wang, and G. Chen, "STAE-YOLO: Intelligent detection algorithm for risk management of construction machinery intrusion on transmission lines based on visual perception," *IET Gener., Transmiss. Distrib.*, vol. 18, no. 3, pp. 542–567, Feb. 2024.

[15] C. Liu, Y. Yao, J. Li, J. Qian, and L. Liu, "Research on lightweight GPR road surface disease image recognition and data expansion algorithm based on YOLO and GAN," *Case Stud. Construct. Mater.*, vol. 20, Jul. 2024, Art. no. e02779.

[16] Y. Bai, J. Yu, S. Yang, and J. Ning, "An improved YOLO algorithm for detecting flowers and fruits on strawberry seedlings," *Biosyst. Eng.*, vol. 237, pp. 1–12, Jan. 2024.

[17] D. P. Carrasco, H. A. Rashwan, M. Á. García, and D. Puig, "T-YOLO: Tiny vehicle detection based on YOLO and multi-scale convolutional neural networks," *IEEE Access*, vol. 11, pp. 22430–22440, 2023.

[18] X. Qian, X. Wang, S. Yang, and J. Lei, "LFF-YOLO: A YOLO algorithm with lightweight feature fusion network for multi-scale defect detection," *IEEE Access*, vol. 10, pp. 130339–130349, 2022.

[19] Z. Liu, Y. Gao, and Q. Du, "YOLO-class: Detection and classification of aircraft targets in satellite remote sensing images based on YOLO-extract," *IEEE Access*, vol. 11, pp. 109179–109188, 2023.

[20] Y. Yang, Z. Miao, H. Zhang, B. Wang, and L. Wu, "Lightweight attention-guided YOLO with level set layer for landslide detection from optical satellite images," *IEEE J. Sel. Topics Appl. Earth Observ. Remote Sens.*, vol. 17, pp. 3543–3559, 2024.

[21] Y. Li, S. Zhang, and W.-Q. Wang, "A lightweight faster-RCNN for ship detection in SAR images," *IEEE Geosci. Remote Sens. Lett.*, vol. 19, 2022, Art. no. 4006105.

[22] F. Fang, L. Li, H. Zhu, and J.-H. Lim, "Combining faster R-CNN and model-driven clustering for elongated object detection," *IEEE Trans. Image Process.*, vol. 29, pp. 2052–2065, 2020.

[23] F. N. Ortataş and M. Kaya, "Performance evaluation of YOLOv5, YOLOv7, and YOLOv8 models in traffic sign detection," in *Proc. 8th Int. Conf. Comput. Sci. Eng. (UBMK)*, Sep. 2023, pp. 151–156.

[24] M. Bakirci and I. Bayraktar, "Boosting aircraft monitoring and security through ground surveillance optimization with YOLOv9," in *Proc. 12th Int. Symp. Digit. Forensics Secur. (ISDFS)*, Apr. 2024, pp. 1–6.

[25] X. Zhu, S. Lyu, X. Wang, and Q. Zhao, "TPH-YOLOv5: Improved YOLOv5 based on transformer prediction head for object detection on drone-captured scenarios," in *Proc. IEEE/CVF Int. Conf. Comput. Vis. Workshops (ICCVW)*, Montreal, BC, Canada, Oct. 2021, pp. 2778–2788.

[26] H. Rezatofighi, N. Tsoi, J. Gwak, A. Sadeghian, I. Reid, and S. Savarese, "Generalized intersection over union: A metric and a loss for bounding box regression," in *Proc. IEEE/CVF Conf. Comput. Vis. Pattern Recognit. (CVPR)*, Long Beach, CA, USA, Jun. 2019, pp. 658–666.

[27] T. -Y. Lin, M. Maire, and S. Belongie, "Microsoft COCO: Common objects in context," in *Proc. ECCV*, Zurich, Switzerland, 2014, pp. 740–755.

[28] D. Arthur and S. Vassilvitskii, "K-means++: The advantages of careful seeding," in *Proc. SODA*, New Orleans, LA, USA, 2007, pp. 1027–1035.

with the School of Innovation and Entrepreneurship, USST. Since 2022, he has been a Professor and the Vice President of the School of Mechanical Engineering, USST. He has been in charge of more than 50 research projects from the government and companies and published more than 80 articles. His research interests include motor and motor control and new energy applications. He won the Third Prize of the Scientific and Technological Progress Award of Zhejiang Province, in 2017, and Shanghai, in 2020.

YIREN LIU was born in China, in 1997. He received the B.Eng. degree from the Department of Electrical Engineering and Its Automation, University of Shanghai for Science and Technology (USST), Shanghai, China, in 2021. He is currently pursuing the M.Eng. degree with the Department of Electrical Engineering, USST. His current research interests include deep learning and arc fault detection.

KUN XIA received the B.Eng. degree in industrial automation and the Ph.D. degree in power electronics and power drives from Hefei University of Technology (HFUT), Hefei, China, in 2002 and 2007, respectively. From 2007 to 2011, he was a Lecturer with the University of Shanghai for Science and Technology (USST), Shanghai, China. From 2011 to 2019, he was an Associate Professor and the Department Head with the Department of Electrical Engineering, USST. From 2015 to 2016, he was also a Visiting Scholar with the Department of Electrical and Computer Engineering, National University of Singapore, Singapore. From 2020 to 2022, he was a Professor and the Vice President

SHUAI YUAN received the B.Eng. degree in materials science and engineering from Southwest Jiaotong University (SWJTU), Chengdu, China, in 2015, and the M.Eng. degree in mechanical engineering from Tiangong University (TJPU), Tianjin, China, in 2018. From 2018 to 2020, she was an Assistant Researcher with Tianjin Sino-German University of Applied Sciences (TSGUAS), Tianjin. Since 2020, she has been an Assistant Experimentalist with the University of Shanghai for Science and Technology (USST), Shanghai, China. She has been in charge of four research projects from the government and companies and published seven articles. Her research interests include mechanical engineering and innovation and entrepreneurship.

• • •